

Spherical Activated Carbon Derived from Spherical Cellulose and Its Performance as EDLC Electrode

Toshiki Tsubota, Daisuke Nagata, Naoya Murakami, Teruhisa Ohno

Department of Applied Chemistry, Faculty of Engineering, Kyushu Institute of Technology, 1-1 Sensuicho, Tobata-ku, Kitakyushu 804-8550, Japan

Correspondence to: T. Tsubota (E-mail: tsubota@che.kyutech.ac.jp)

ABSTRACT: Spherical activated carbons (ca. 30–100 μm in diameter) were synthesized from commercial spherical cellulose beads. The addition of guanidine phosphate was performed as the pretreatment, and CO_2 activation was applied for enhancing the specific surface area. The addition of guanidine phosphate drastically improved the yield of carbon during the activation process. The specific surface area reached $1545 \text{ m}^2 \text{ g}^{-1}$ for the sample heat-treated at 850°C for 1 h in flowing N_2 and continuously for 3 h in flowing CO_2 activation. The calculated capacitance values per area (F m^{-2}) for the pore size of less than 1 nm was large in the case of small current density. The distortion of the solvation shell could be the reason for the large capacitance value for the small pore size of less than 1 nm. © 2014 Wiley Periodicals, Inc. *J. Appl. Polym. Sci.* **2014**, *131*, 40950.

KEYWORDS: applications; cellulose and other wood products; electrochemistry; flame retardance; porous materials

Received 5 March 2014; accepted 1 May 2014

DOI: 10.1002/app.40950

INTRODUCTION

Recently, many research studies related to electrical energy storage devices, such as the lithium-ion secondary battery, have been performed for performance improvement. Electrochemical capacitors, such as the electrical double layer capacitor (EDLC), are also an electrical energy storage device. The electrochemical capacitors have a few advantages over the other devices, for example, a high-power charge-discharge performance. However, because the density of the stored energy of the electrochemical capacitors is lower than that of lithium-ion secondary battery, the change in the density should be desired for the application of electrochemical capacitors. The density of the stored energy for an electrochemical capacitor should depend on the property of the electrode material. Therefore, many reports on electrochemical capacitors are related to improvement of the electrode material.

So far, some concepts for the EDLC electrode material, such as a high specific surface area, enhancement of mesopores (2–50 nm), addition of heteroatoms, introduction of ultramicropore (less than 0.7 nm), etc., have been proposed in order to improve the capacitance value, which is related to the amount of the stored electrical energy. As for the addition of heteroatoms, some papers reported that the addition of nitrogen atoms is effective for improving the capacitance^{1–4} although the effect

of the addition has been under discussion.⁵ As for the introduction of ultramicropore, some paper reported the high capacitance values for ultramicropore.^{6,7}

The chemical structure of polysaccharide such as cellulose is $(\text{C}_6\text{H}_{10}\text{O}_5)_n$. The yields of the carbon material derived from polysaccharide are not high because the percentage of oxygen atoms is relatively high in the chemical structure. Therefore, polysaccharide may not be an advantageous precursor from the aspect of the raw material for a carbon material. However, polysaccharide is suitable as the precursor of a carbon material from the aspect of environmental harmony because polysaccharide is a carbon neutral material. So far, several kinds of biomass, which contains cellulose, have been studied as the precursors for the carbon material of the EDLC electrode.⁸

Some researchers reported the effect of iodine treatment on the carbonization of polysaccharide.^{9,10} Carbon materials derived from polysaccharide have been studied as the absorbents for wastewater treatment.¹¹ However, most of these carbon materials have relatively low specific surface areas. We have already reported that the addition of guanidine phosphate is effective for the improvement of the capacitive performance of the carbon material derived from starch.^{12–14} It could be presumed that the addition of guanidine phosphate to cellulose is effective for the improvement of the capacitive performance because

Additional Supporting Information may be found in the online version of this article.

© 2014 Wiley Periodicals, Inc.

cellulose is a type of polysaccharide and because one of the presumed reasons for the improvement is the introduction of the N atoms in the sample. Moreover, it is known that guanidine phosphate is a flame retardant for cellulose materials. Because the mechanism of flame retardance of guanidine phosphate resulted in the enhancement of the amount of char,¹⁵ that is, carbon material, we could expect an increased yield of the produced carbon material. The addition of guanidine phosphate before the heating process to cellulose is simple, easy, safe, and inexpensive. Therefore, this method should be important for the synthesis of a carbon material in practical use. If the method proposed in this study was effective for the improvement of the capacitance performance, then we can produce a high performance material at a low price.

In general, the shape of carbon particle for an electrochemical capacitor was not considered because the sizes of ions are much smaller than that of the carbon particles. However, in some research studies, spherical carbon was used for the electrochemical capacitor.^{16–22} If uniformly sized spherical activated carbon were applied for the EDLC electrode, uniform voids should be formed among the spheres. The solvent should quickly penetrate via the voids because the size of the voids is relatively large. The quick penetration of the solvent could be advantageous to diffuse the ions, which could result in a high capacitance value at a high current density. Zheng et al. used spherical carbon beads derived from coal tar pitch as the negative electrode for an electrochemical capacitor.¹⁶ Zhou et al. investigated the capacitance property of a spherical carbon aerogel synthesized using $Mg(OH)_2$.¹⁸ Campos et al. reported slurry containing spherical carbon as a flowable electrode in an electrochemical flow capacitor.¹⁷ Liu et al. reported the property and the performance of mesoporous carbon microspheres which were partially graphitized by a nickel catalyst.¹⁹ In this study, activated spherical carbon was synthesized from cellulose beads treated with guanidine phosphate and CO_2 activation, and the properties related to the capacitance were investigated in detail.

EXPERIMENTAL

Commercial spherical cellulose beads (D-100, Daito Kasei Kogyo), the average diameter of which is 100 μm , was used as the carbon source, and guanidine phosphate (Tokyo Chemical Industry) was used as the additive in this study. The guanidine phosphate, the amount of which was 5 wt % versus the spherical cellulose beads, was first dissolved in distilled water. The spherical cellulose beads were then suspended in the aqueous solution. The suspension was dried in a dryer. After the drying, the spherical cellulose beads were placed in a quartz boat, and then the quartz boat was set in a tubular furnace for the heat treatment. The spherical cellulose beads were carbonized at 850°C for 1 h in flowing N_2 , and continuously heated for activation at 850°C for x min ($x = 10 - 240$) in flowing CO_2 .

The TG-DTA measurements (Rigaku Corporation, TG-TDA8120H) were performed for thermal analysis. The microstructure of the samples was investigated using an FE-SEM (JEOL, JSM-6320F). The N_2 adsorption isotherms (Quantachrome Instruments, NOVA4200e) were measured for estimation

of the pore size distribution and BET specific surface area. Another apparatus (Quantachrome, Autosorb-1C/MS) was used for the measurements of the lower relative pressure in detail. The CHN corder (Yanaco New Science, MT-5) was used to estimate the percentages of the C atoms, the H atoms, the N atoms in the samples. The XPS measurements (Kratos Analytical Limited, AXIS-NOVA) were used for confirming the existence of the N atoms and the P atoms in the samples.

The synthesized carbon material was mixed with PTFE in order to form a sample sheet. The weight ratio of PTFE to the carbon material was 1/99. A few drops of N-methylpyrrolidone were used for the homogeneous dispersion of the PTFE. The sheet sample, the thickness of which was ca. 0.5 mm, was cut in the size of 20 mm \times 8 mm for the electrochemical measurements, such as cyclic voltammetry and charge–discharge test. These electrochemical measurements were performed in a three-electrode cell using a potentiostat/galvanostat (TOYO Corporation, VersaSTAT3). A 1M H_2SO_4 aqueous solution, which was bubbled with N_2 gas before the electrochemical measurements, was used as the electrolyte. A Pt plate was used as the counter electrode, the sheet sample, which was pressed on another Pt plate in the cell was used as the working electrode, and a Ag/AgCl electrode was used as the reference electrode. The capacitance values were calculated from the charge process data of the charge process.

RESULTS AND DISCUSSION

Preparation of the Samples

The yields, which were calculated from the W_{after}/W_{before} value (W_{after} and W_{before} are the weight of the sample after the heat treatment and that before the heat treatment, respectively), are shown in Figure 1. When the activation time was 0, that is, the sample was heated for 1 h in flowing N_2 , the yield of the spherical cellulose sample was ca. 12 wt %. On the other hand, the yield of the sample added with guanidine phosphate was ca. 30 wt %. The values of the yield drastically increased with the addition of the guanidine phosphate. The results of the TG-DTA measurements are shown in Supporting Information Figure S1. As shown in the graph, the temperature dropped the weight decreased with the addition of guanidine phosphate. Because it is known that guanidine phosphate as a flame retardant decreases the temperature for the heat decomposition of the endocyclic C–O bond, the decrement of the temperature for the rapid drop of the weight should be the effect of guanidine phosphate. The temperatures dropped the weight much lower than the heat treatment temperature applied in this study, that is, 850°C. Therefore, spherical cellulose should be carbonized under the condition of this study. The chemical formula of cellulose is $(C_6H_{10}O_5)_n$. That is, the proportion of the number of oxygen atoms to that of carbon atoms is high. This could be the reason for the relatively small yield of the sample with no added guanidine phosphate. It is known that guanidine phosphate acts as a flame retardant for cellulose.^{23–26} It is reported that the addition of guanidine phosphate to cellulose affects the carbonization process of the cellulose.²³ The proposed mechanism is that the C–O bond in the ring structure of cellulose is preferentially cut by the catalysis of guanidine phosphate, resulting in the enhancement of the char (carbon material). This

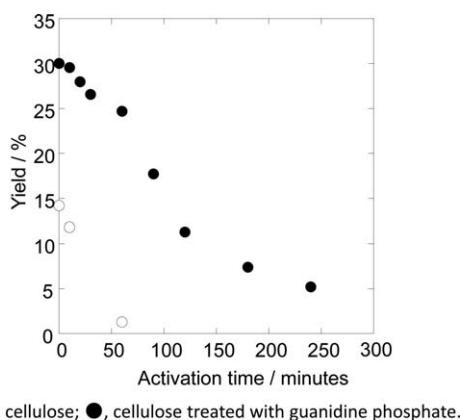


Figure 1. Yields after activation process. ○, cellulose; ●, cellulose treated with guanidine phosphate.

should be the reason for the improvement of the yield at no CO_2 activation. When guanidine phosphate was applied as a flame retardant, in general the experiments for the heat treatment were usually performed less than 500°C in air. Moreover, because the purpose of these experiments is not the synthesis of the carbon material by the heat treatment, but the analysis of the reaction during the heating process, there were no results for the CO_2 activation of the char (carbon material). The yield of the sample after CO_2 activation process drastically improved with the addition of guanidine phosphate. It should be noted from the experimental data of this study that the addition of guanidine phosphate was effective for the changing the yield of the activation process. Because the enhancement of the yield is valuable for cost-down of the industrial product of activated carbon, the addition of guanidine phosphate should be interesting. Therefore, the properties of the sample with added guanidine phosphate were studied in detail.

Optical microscope and SEM images of the samples with added guanidine phosphate are shown in Figure 2. The spherical shape was maintained during the heating process in the flowing N_2 and the activation process in flowing CO_2 although the diameters of the spheres slightly decreased with increasing the activation time. However, the surface roughness increased with the increasing activation time. The reason for the surface roughness should be the activation reaction with CO_2 .

The percentage of the elements estimated from XPS measurements are listed in Table I. It should be noted that both the P atoms and the N atoms existed in the samples treated with no activation process. Moreover, the sample after the activation process also contained both elements. Because some of carbon material containing the N atom had high performance as EDLC electrode, the condition of the nitrogen in carbon material was investigated by XPS.²⁷ The XPS spectra of narrow scan for N are shown in Figure 3. There are some peaks in the spectra. The calculated percentages of the condition of N from the separated peaks are listed in Table II. The peaks are assigned by reference to the reported papers.²⁷ The two peaks at lower binding energy should be assigned to pyrrolic N and pyridinic N could because the peak positions were almost similar to the reported positions.²⁷ The two peaks at higher binding energy could be

assigned to N-oxide and quaternary N although the peak positions are slightly higher than the reported positions.²⁷ The reason for the shifting to higher positions is unclear. Before the activation with CO_2 , the percentage of quaternary nitrogen was more than 50%. On the other hand, after the activation process, the percentage of quaternary nitrogen was less than 35%. The total amount of N in the sample decreased with CO_2 activation. Therefore, the reason for the decrement of the percentage of quaternary nitrogen may not be the change from quaternary nitrogen to pyrrolic N but be the decrement of quaternary N. Therefore, the stability of the N atom against CO_2 activation should depend on the structure containing the N atom.

Capacitance Properties of the Samples

We have already reported that the addition of guanidine phosphate to starch or cellulose is effective for improving the capacitance value of the carbon material synthesized by heat treatment.^{12–14} The current density dependence on the capacitance values are shown in Figure 4. The capacitance values of the charge process and the discharge process are shown in the Supporting Information Figure s2. The CV graph (1 mV s^{-1}) and the charge–discharge graph (10 mA g^{-1}) for the sample activated for 3 h was written in Supporting Information Figure s3. The shape of the CV graph is nearly rectangle, and that of the charge–discharge graph is nearly isosceles triangle. The graphs are typical shapes for electrical double layer capacitor. The capacitance values drastically increased with the increasing activation time of CO_2 , and then the maximum capacitance values were achieved when the activation time was 180 min.

All the N_2 adsorption isotherms of the samples with added guanidine phosphate were the “I” type defined by IUPAC (as shown in Supporting Information Figure s4). The shape of “I” type should mean that there are many micropores (less than 1 nm) in the sample. To analyze micropore, the measurements of the lower relative pressure were performed as shown in Supporting Information Figure s5. Because the volume of the adsorbed N_2 of the sample for Supporting Information Figure s5 was larger than that for Supporting Information Figure s4, it can be presumed that the value of specific surface area was sensitive to the atmosphere of carbonization process. (Small amount of air, which could act as an activation agent, might leak in the tubular furnace for the sample of Supporting Information Figure s5.) However, the experimental data should indicate that most of the pores for the samples are ultramicropore (less than 0.7 nm). The activation time dependence on the BET specific surface area is shown in Figure 5. The specific surface area increased with the increasing activation time up to 180 min. The maximum value of the specific surface area was $1545 \text{ m}^2 \text{ g}^{-1}$ for the sample treated for 180 min.

The DFT method was performed in order to evaluate the micropore distribution (shown in Supporting Information Figure s6). The activation time dependence on the micropore distribution can be classified as follows:

1st step (0–60 min): the formation of the microsize pore

2nd step (120–240 min): the enhancement of the pore size

During the 1st step, the pore volume of the micropore (less than 1 nm) increased with increasing the activation time.

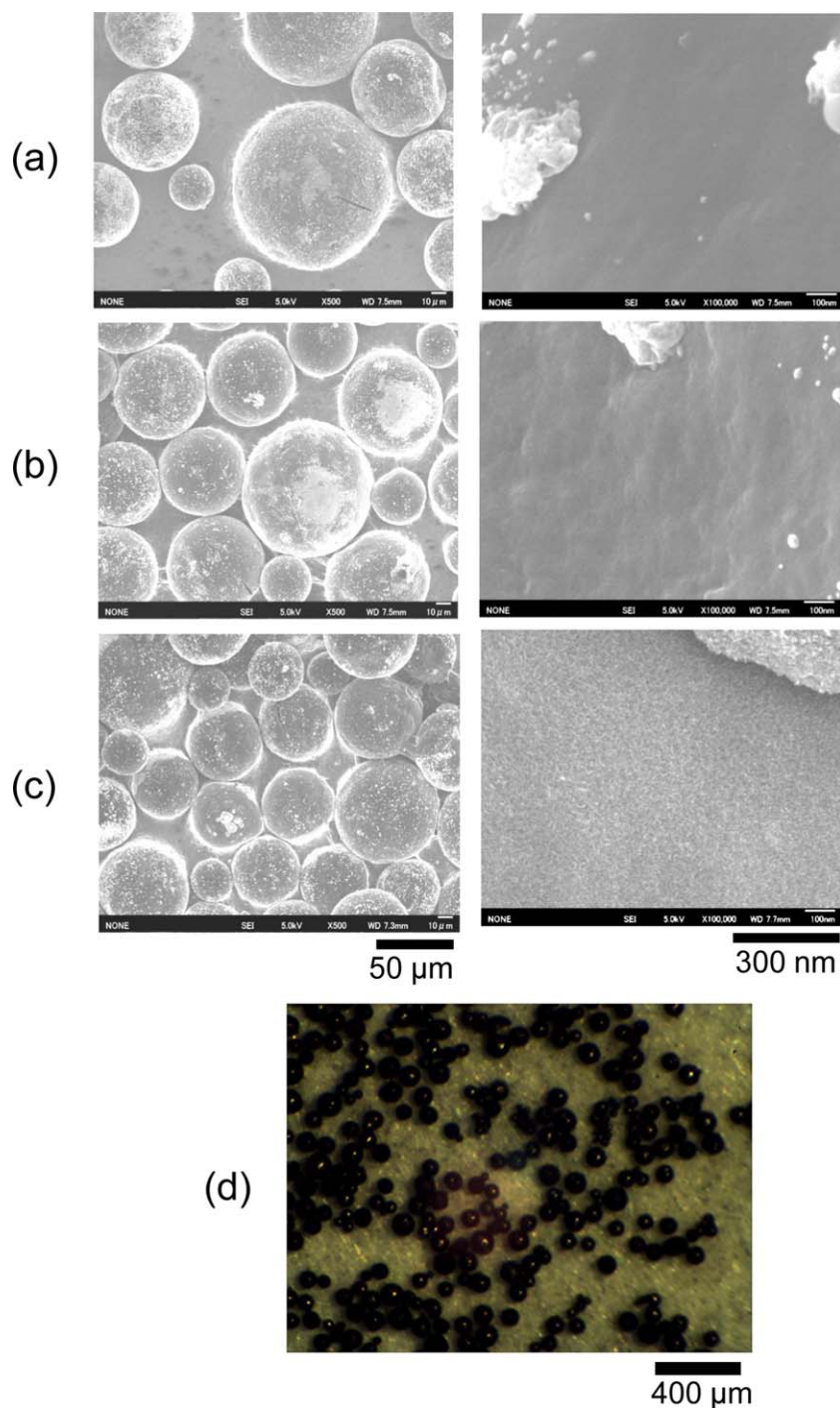


Figure 2. Optical microscope and SEM images of the samples treated at 850°C for 1 h in N_2 flow and then continuously 850°C for x h in CO_2 flow. (a), $x = 0$; (b), $x = 10$; (c), $x = 180$. [Color figure can be viewed in the online issue, which is available at wileyonlinelibrary.com.]

Therefore, the new microsize pore should form in the sample during the activation process. The enhancement of the specific surface area with the CO_2 activation for 30 min should be caused by the increment of micropores. During the 2nd step, the peak at less than 1 nm decreased and the peak at ca. 1.8 nm increased with the increasing activation time. Therefore, the pore size increased with the increasing activation time during the 2nd step. Based on the micropore distribution of the

Table I. The Percentages of the Elements Estimated from XPS Measurements

CO_2 activation time (hour)	C (atomic %)	O (atomic %)	N (atomic %)	P (atomic %)
0	84.69	10.42	2.77	2.12
3	72.54	20.45	2.09	4.92

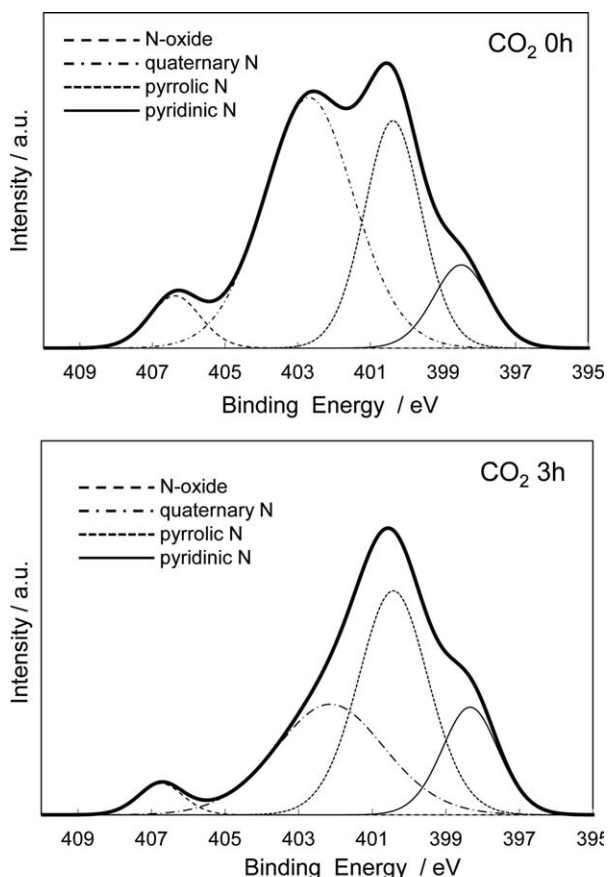


Fig. 3 The XPS spectra of narrow scan for N.

Figure 3. The XPS spectra of narrow scan for N.

samples activated for 120–240 min. the pore size area should be divided into four groups, that is, less than 1 nm, 1–1.5 nm, 1.5–2 nm, and more than 2 nm. When carbon sphere derive from phenol resin, which was glass-like carbon, was activated air, the amount of micropore decreased and that of mesopore increased at the long activation process.²⁸ The reason for the phenomena was presumed that the change in pore volumes gradually enlarged the pore size from micropore to mesopore. This mechanism could be explained the experimental results in this study.

The measured capacitance value, C_{total} [F g^{-1}], can be expressed as follows²⁹:

$$C_{\text{total}} = C_{-A} * S_{-A} + C_{A-} * S_{A-} \quad (1)$$

where C_{-A} [F m^{-2}] is the capacitance value derived from the pore whose size is less than A nm, C_{A-} [F m^{-2}] is the capacitance value derived from the pore whose size is greater than A

nm, S_{-A} [$\text{m}^2 \text{g}^{-1}$] is the specific surface area derived from the pore whose size is less than A nm, and S_{A-} [$\text{m}^2 \text{g}^{-1}$] is the specific surface area derived from the pore whose size is greater than A nm.

From Eq. (1),

$$C_{\text{total}}/S_{-A} = C_{-A} * (S_{-A}/S_{A-}) + C_{A-} \quad (2)$$

Therefore, C_{-A} and C_{A-} can be estimated from the relation between C_{total}/S_{-A} and S_{-A}/S_{A-} .

We can write the following equations by modifying of Eq. (1):

$$C_{\text{total}} = C_{-A1} * S_{-A1} + C_{A1-A2} * S_{A1-A2} + \dots + C_{An-} * S_{An-} \quad (3)$$

$$C_{-A2} * S_{-A2} = C_{-A1} * S_{-A1} + C_{A1-A2} * S_{A1-A2} \quad (4)$$

$$C_{A1-} * S_{A1-} = C_{A1-A2} * S_{A1-A2} + C_{A2-} * S_{A2-} \quad (5)$$

where C_{-A1} [F m^{-2}] is the capacitance value derived from the pore whose size is less than A1 nm, C_{A1-A2} [F m^{-2}] is the capacitance value derived from the pore whose size is from A1 nm to A2 nm, C_{An-} [F m^{-2}] is the capacitance value derived from the pore whose size is greater than An nm, S_{-A1} [$\text{m}^2 \text{g}^{-1}$] is the specific surface area derived from the pore whose size is less than A1 nm, S_{-A2} [$\text{m}^2 \text{g}^{-1}$] is the specific surface area derived from the pore whose size is less than A2 nm, S_{A1-A2} [$\text{m}^2 \text{g}^{-1}$] is the specific surface area derived from the pore whose size is from A1 nm to A2 nm, and S_{An-} [$\text{m}^2 \text{g}^{-1}$] is the specific surface area derived from the pore whose size is greater than An nm.

In this study, the pore sizes for Eq. (3) were determined from the experimental results of pore size distributions.

$$C_{\text{total}} = C_{-1} * S_{-1} + C_{1-1.5} * S_{1-1.5} + C_{1.5-2} * S_{1.5-2} + C_{2-} * S_{2-} \quad (6)$$

$$C_{1-1.5} * S_{1-1.5} = C_{-1.5} * S_{-1.5} - C_{-1} * S_{-1} = C_{1-} * S_{1-} + C_{1.5-} * S_{1.5-} \quad (7)$$

$$C_{1.5-2} * S_{1.5-2} = C_{-2} * S_{2-} - C_{-1.5} * S_{-1.5} = C_{1.5-} * S_{1.5-} + C_{2-} * S_{2-} \quad (8)$$

In order to calculate these capacitance values, we used the experimental data of C_{total} , S_{-1} , $S_{1-1.5}$, $S_{1.5-2}$, and S_{2-} . (The method for the calculation is detailed in the Supporting Information.) The calculated results are shown in Figure 6. The order of the calculated capacitance values per area should be reasonable because these values are comparable with reported values.^{30–33} The values should indicate that most part of the capacitance was assigned to the capacitance of electrical double layer.³⁴ That is, the contribution of the structure containing N could be small. Therefore, main reason for the enhancement of the capacitance values should be not the effect of the N atom but the increment of specific surface area. For the 1000 mA g^{-1} current density, the calculated capacitance value decreased with the decreasing pore size. The decrease in the capacitance value

Table II. The Calculated Percentages of the Condition of N from the Separated Peaks

CO ₂ activation time (hour)	N-oxide (atomic %) 406.3–406.8 eV	Quaternary N (atomic %) 402.1–402.7 eV	Pyrrolic N (atomic %) 400.4 eV	Pyridic N (atomic %) 398.3 eV
0	6.21	52.51	30.42	10.86
3	3.98	34.10	44.66	17.26

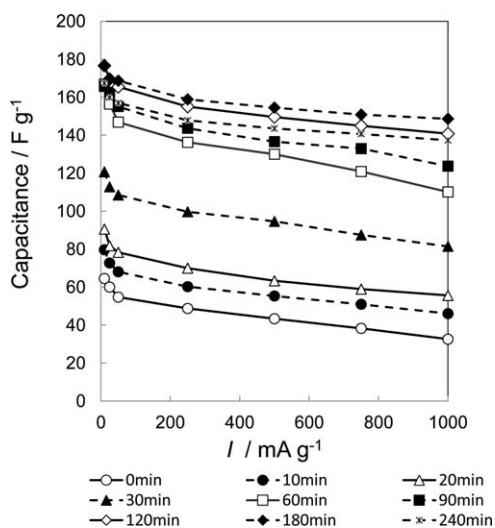


Figure 4. This density dependence on the capacitance values.

could be explained by the diffusion of the ion species. Because the ion species should be difficult to diffuse through small pores, the capacitance value could decrease with the decreasing pore size. For the 10 mA g^{-1} current density, the pores of less than 1 nm in pore size had the highest capacitance value.

It was reported that the pore size less than 1 nm had the highest capacitance value per area for a non-aqueous electrolyte^{30–32} and for an aqueous electrolyte.³³ In the pores near the size of the solvation shell, the solvation shell became distorted. Such a distortion would allow a closer approach of the ion center to the electrode surface. Because the capacitance value is inversely proportional to the distance between the ion and the electrode surface, the capacitance value should be improved. We can estimate the size of the SO_4^{2-} ion from the covalent radius of oxygen (0.074 nm) and the distance between the S atom and the O atom in the SO_4^{2-} ion (ca. 0.15 nm). The estimated size of the SO_4^{2-} ion could be ca. 0.4–0.5 nm. Therefore, the change in the capacitance value for the pore size less than 1 nm could be explained by the above phenomenon. The capacitance values per area were independent of the current density for the charge–discharge process

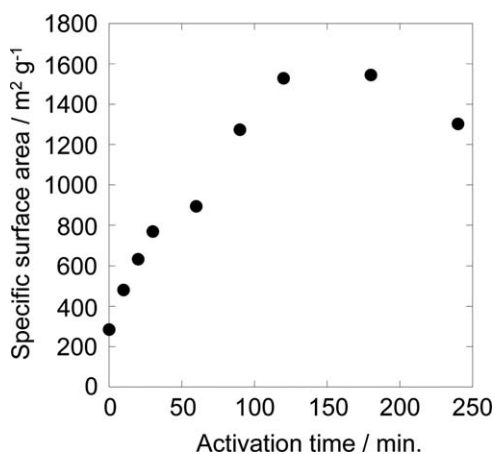


Figure 5. The activation time dependence on the BET specific surface area.

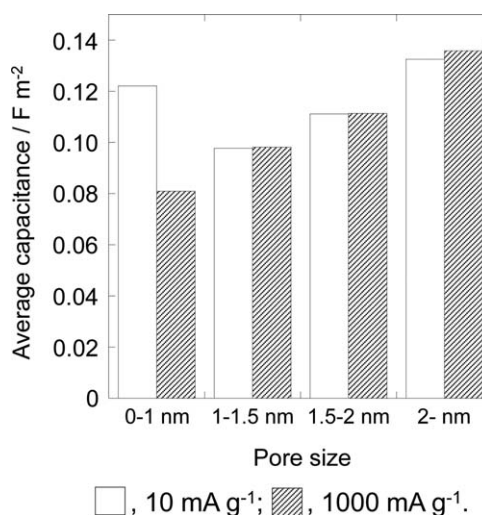


Figure 6. Average capacitance values.

except for the pore size of less than 1 nm. This should mean that the interaction between the electrode surface and the ions was independent of the current density for the charge–discharge process except for the pore size of less than 1 nm. However, when a high current density (1000 mA g^{-1}) was applied to the charge–discharge process, the capacitance value per area decreased with the decreasing pore size. The diffusion speed of the ions should be low in the small pores. This could be the reason for the low capacitance value per area for the small pore size.

CONCLUSIONS

Spherical activated carbon beads were synthesized from spherical cellulose beads treated with guanidine phosphate. The yield of the produced carbon material increased with the addition of the guanidine phosphate. The N atoms and the P atoms, which should come from the guanidine phosphate, existed in the synthesized sample. The specific surface area of the sample increased with the CO_2 activation process, and the maximum value of the specific surface area was $1545 \text{ m}^2 \text{ g}^{-1}$. The pore size dependences of the capacitance value per area were estimated from the measured capacitance values and the measured pore size distribution. Although most of the capacitance values per area were independent of the current density for the charge–discharge process, the capacitance values per area for the pore size of less than 1 nm decreased with the increasing current density. The change in the capacitance value for the small pore size could be explained by distortion of the solvation shell, and the decrease in the capacitance value at a high current density could be related to the diffusion speed of the ions.

REFERENCES

- Kodama, M.; Yamashita, J.; Soneda, Y.; Hatori, H.; Kamegawa, K. *Carbon* **2007**, *45*, 1105.
- Frackowiak, E.; G. Lota, G.; Machnikowski, J.; Vix-Guterl, C.; Beguin, F. *Electrochem. Acta* **2006**, *51*, 2209.
- Hulicova, D.; Yamashita, Y.; Soneda, Y.; Hatori, H.; Kodama, M. *Chem. Mater.* **2005**, *17*, 1241.

4. Xiong W.; Liu M.; Gan L.; Lv Y.; Xu Z.; Hao Z.; Chen L. *Colloid Surface A* **2012**, *411*, 34.
5. Kwon, T.; Nishihara, H.; Itoi, H.; Yang, Q.-H.; Kyotani, T. *Langmuir* **2009**, *25*, 11961.
6. Chmiola, J.; Yushin, G.; Gogotsi, Y.; Porter, C.; Simon, P.; Taberna, P. L. *Science* **2006**, *313*, 1760.
7. Zhao, Y.; Liu, M.; Gan, L.; Ma, X.; Zhu, D.; Xu, Z.; Chen, L. *Energy Fuels* **2014**, *28*, 1561.
8. Kalyani, P.; Anitha, A. *Int. J. Hydrogen Energy* **2013**, *38* 4034.
9. Miyajima, N.; Ishikawa, N.; Sakane, H.; Tanaike, O.; Hatori, H.; Akatsu, T.; Yasuda, E. *Thermochim. Acta* **2010**, *498*, 33.
10. Kyotani, M.; Matsushita, S.; Kimura, S.; Akagi, K. *J. Anal. Appl. Pyrol.* **2012**, *95*, 14.
11. Crini, G. *Prog. Polym. Sci.* **2005**, *30*, 38.
12. Tsubota, T.; Yamaguchi, T.; Wang, C. S.; Miyachi, Y.; Murakami, N.; Ohno, T. *J. Power Sources* **2013**, *227*, 24.
13. Tsubota, T.; Wang, C.S.; Murakami, N.; Ohno, T. *J. Power Sources* **2013**, *225*, 150.
14. Tsubota, T.; Miyachi, Y.; Murakami, N.; Ohno, T. *J. Power Sources* **2011**, *196*, 5769.
15. Granzow, A. *Acc. Chem. Res.* **1978**, *11*, 177.
16. Zheng, C.; Gao, J. C.; Yoshio, M.; Qi, L.; Wang, H. Y. *J. Power Sources* **2013**, *231*, 29.
17. Campos, J. W.; Beidaghi, M.; Hatzell, K. B.; Dennison, C. R.; Musci, B.; Presser, V.; Kumbur, E. C.; Gogotsi, Y. *Electrochim. Acta* **2013**, *98*, 123.
18. Zhou, J. H.; Ji, Y. J.; He, J. P.; Zhang, C. X.; Zhao, G. W. *Microporous Mesoporous Mater.* **2008**, *114*, 424.
19. Liu, M.; Gan, L.; Xiong, W.; Zhao, F.; Fan, X.; Zhu, D.; Xu, Z.; Hao, Z.; Chen, L. *Energy Fuels* **2013**, *27*, 1168.
20. Kim, H.; Fortunato, M. E.; Xu, H.; Bang, J. H.; Suslick, K. S. *J. Phys. Chem. C* **2011**, *115*, 20481.
21. Xiong, W.; Liu, M.; Gan, L.; Lv, Y.; Li, Y.; Yang, L.; Xu, Z.; Hao, Z.; Liu, H.; Chen, L. *J. Power Sources* **2011**, *196*, 10461.
22. Wang, X.; Liu, L.; Wang, X.; Bai, L.; Wu, H.; Zhang, X.; Yi, L.; Chen, Q. *J. Solid State Electrochem.* **2011**, *15*, 643.
23. Granzow, A. *Acc. Chem. Res.* **1978**, *11*, 177.
24. Lecoq, E.; Vroman, I.; Bourbrigit, S.; Delobel, R. *Polym. Degrad. Stab.* **2006**, *91* 1909.
25. Gao, M.; Sun, C.; Zhu, K. *J. Therm. Anal. Calorim.* **2004**, *75*, 221.
26. Gao, M.; Ling B.; Yang S.; Zhao, M. *J. Anal. Appl. Pyrol.* **2005**, *73*, 151.
27. Konno, H.; Ito, T.; Ushiro, M.; Fushimi, K.; Azumi, K. *J. Power Sources* **2010**, *195*, 1739.
28. Inagaki, M. *New Carbon Mater.* **2009**, *24*, 193.
29. Shi, H. *Electrochim. Acta* **1996**, *41*, 1633.
30. Chmiola, J.; Yushin, G.; Gogotsi, Y.; Portet, C.; Simon P.; Taberna, P. L. *Science* **2006**, *22*, 1760.
31. Huang, J.; Sumpter, B. G.; Meunier, V. *Chem. A Eur. J.* **2008**, *14*, 6614.
32. Huang, J.; Sumpter, B. G.; Meunier, V. *Angew. Chem. Int. Ed.* **2008**, *47*, 520.
33. Simon, P.; Gogotsi, Y. *Phil. Trans. Roy. Soc. A* **2010**, *368*, 3457.
34. Centeno, T. A.; Stoeckli, F. *Electrochim. Acta* **2006**, *52* 560.